

Coronal flux tube illuminated by strong shock spot: New Year's Eve solar eruption of 2023-Dec-31

Illya Plotnikov¹  · Alexis Rouillard¹  ·
 Athanasios Kouloumvakos²  ·
 Immanuel Jebara³ 

© The author(s) ••••

Abstract Powerful solar eruptions are known to produce fast and wide shock waves in the solar corona and inner heliosphere. The relationship between the coronal shock waves, solar energetic particles and different types of radio emission is a subject of long-lasting research activity. In this work, we perform a case study of 31 December 2023 eruption that occurred near eastern limb of the Sun. It produced a X5.0 class X-ray flare, a global EUV wave, a fast ~ 3000 km/s Coronal Mass Ejection, strong radio emissions (including several type III and type II bursts), solar energetic particles in-situ, and long duration high-energy gamma-ray emission. We employ a technique that combines the reconstructed coronal shock from observations with background coronal MHD simulations to produce shock-mediated synthetic radio spectrum, assuming local emission at plasma frequency. We show that transient high Mach number and quasi-perpendicular coronal shock region explains both a “hot flux tube” precursor seen in EUV observations and reverse drifting radio spectral features observed by ground-based facilities. The occurrence of this evanescent strong shock patch was observed when it propagated across pseudo-streamer’s cusp where the magnetic field was particularly low. We also find evidence that, at higher coronal altitudes, the low-frequency type II radio burst detected by several spacecraft, is triggered by the interaction of the shock with the heliospheric current sheet. This study provides additional evidence that high- M_A regions of coronal shock surface are instrumental in energetic particle phenomenology.

Keywords: Corona, Structures; Radio Bursts, Dynamic Spectrum

✉ I. Plotnikov
illya.plotnikov@irap.omp.eu

¹ IRAP, Université de Toulouse / Observatoire Midi-Pyrénées, France

² The Johns Hopkins University Applied Physics Laboratory, Laurel, MD 20723, USA

³ Department of Physics and Astronomy, University of Turku, 20500 Turku, Finland

1. Introduction

Strong solar eruptions are known to produce bright flares and drive fast and wide collisionless shock waves in the solar corona and beyond. Both flares (along with large and dynamic coronal loops) and shocks are widely recognized as efficient non-thermal particle accelerators. However, the main mechanism and source of the most energetic solar particles which are produced during the early phases of the eruption (when all potential sources are still close to each other in low corona) remain debated.

Since the advent of multi-point solar observations in remote-sensing imaging (particularly STEREO mission; Kaiser et al. 2008), it became possible to systematically track and triangulate the propagation of shock waves in the solar corona (e.g., Kwon, Zhang, and Olmedo 2014; Rouillard et al. 2016; Kouloumvakos et al. 2019). Radio observations are long known to be valuable diagnostics of shocks in the corona since they can be associated with the electron acceleration at shock waves (see Klein 2021, for recent review). They are commonly used to track regions of type II emissions and localize where coronal shocks are strong, super-critical and often quasi-perpendicular (e.g., Zucca et al. 2018; Morosan et al. 2019; Kouloumvakos et al. 2021; Jebaraj et al. 2021). These studies generally rely on co-temporality and co-location of reconstructed shock wave regions and radio emissions, especially highlighting the region where the shock interacts with a coronal streamer or Heliospheric Current Sheet (e.g., Cho et al. 2008; Magdalenić et al. 2014; Jebaraj et al. 2020; Frassati et al. 2022; Koval et al. 2023).

In a series of recent studies, using spacecraft that had a close magnetic connection to the eruptive region, it was shown that the same part of the shock are responsible for both metric to decametric solar radio emissions and in situ energetic electrons (Morosan et al. 2022, 2024, 2025; Jebaraj et al. 2023a; Rodríguez-García et al. 2025). Additionally to evidence of energetic particle acceleration in the complex post-flaring loops beneath the expanding shock (e.g., Klein et al. 2005, 2022, 2024), these studies show that strong shock regions in the low solar corona also accelerate electrons efficiently and are the source of their escape into space as well as precipitation towards the solar surface, depending on magnetic connectivity of the accelerating shock region (see, e.g., Mann et al. 2018; Wu et al. 2021, for theoretical model).

In this work, we study radio and EUV signatures of the coronal shock during solar eruption of 31 December 2023. For this event, the radio observations showed that the type II radio burst exhibited an unusual hotspot with a reverse drift and EUV images showed a transient precursor brightening. Both features are not typical and we further explore possible explanations.

Using multi-point EUV and white-light observations we reconstruct the spatial evolution of the coronal shock, which is found to be very fast; reaching 3500 km/s at peak. The reconstruction is then coupled with MHD simulation of the solar corona. Using the technique of Kouloumvakos et al. (2021) and Jebaraj et al. (2021) that produces shock-mediated synthetic radio spectrum, we present evidence that one evanescent particularly strong shock “patch” along its Earth-directed flank was responsible for “hotspot” radio emission feature and for the transient brightening of a localized upstream flux tube observed in EUV.

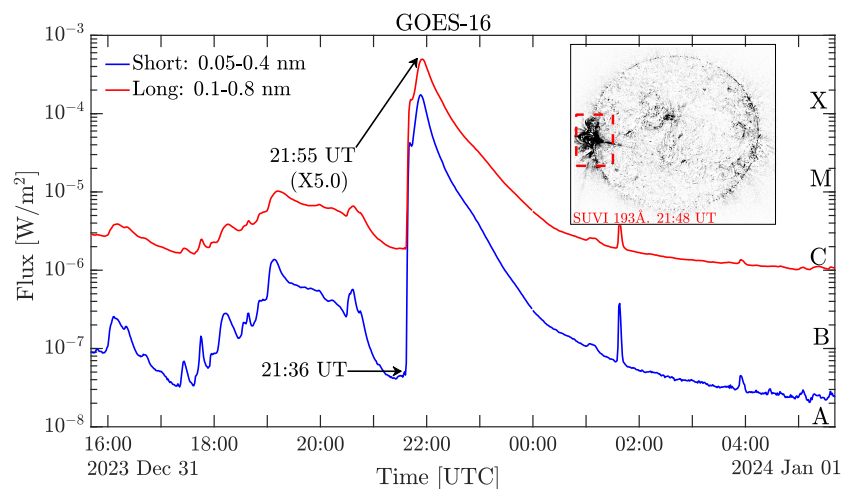


Figure 1. GOES-16 soft X-ray observations from 2023/12/31 to 2024/01/01. The X5.0 flare started at 21:36 UT and peaked at 21:55 UT (indicated by arrows). The inset image displays the GOES-16/SUFI running-difference image at 193 Å wavelength from 21:48 UT and 21:44 UT images. The flaring region at the eastern edge of the Sun is highlighted with red dashed box.

The article is organized as follows. In section 2 we present an overview of the solar eruption observations. section 3 presents the coronal shock reconstruction using remote-sensing EUV and white-light observations. In section 4 we present the results combining observations and shock modeling. Discussion and conclusions are presented in section 5.

2. Overview of the Solar Eruption

On 31 December 2023 a strong solar eruption was observed by various observatories after 21:35 UT originating from the NOAA Active Region (AR) 13536 located at Stonyhurst heliographic latitude $+4^\circ$ and longitude -76° (N04E76) as seen from Earth viewpoint. The corresponding Carrington Longitude and Latitude were 152° and 4° , respectively. A large X-ray flare was recorded by GOES-16/17 mission, starting at 21:36 UT and peaking at 21:55 UT at X5.0 level (see the light-curve in Figure 1). Making this flare the largest of Solar Cycle 25 by the time of eruption.

As common for largest flares, it was accompanied by a global coronal pressure wave surrounding a set of bright coronal loops (Veronig et al. 2010; Warmuth 2015). The wave expansion was observed at Extreme Ultra Violet (EUV) wavelengths by SDO/AIA (Lemen et al. 2012) and STEREO-A/EUVI (Howard et al. 2008). Briefly after the initial phase of the flare, a fast CME lift-off was seen by white-light coronagraphs onboard SOHO (i.e., LASCO-C2 and C3; Brueckner et al. 1995) and STEREO-A (i.e., STA/COR2; Howard et al. 2008). The CME first appeared in LASCO-C2 between 21:48 UT and 22:00 UT and in STA/COR2 field-of-view between 21:38 UT and 21:53 UT. A selection of STA/EUVI (panel

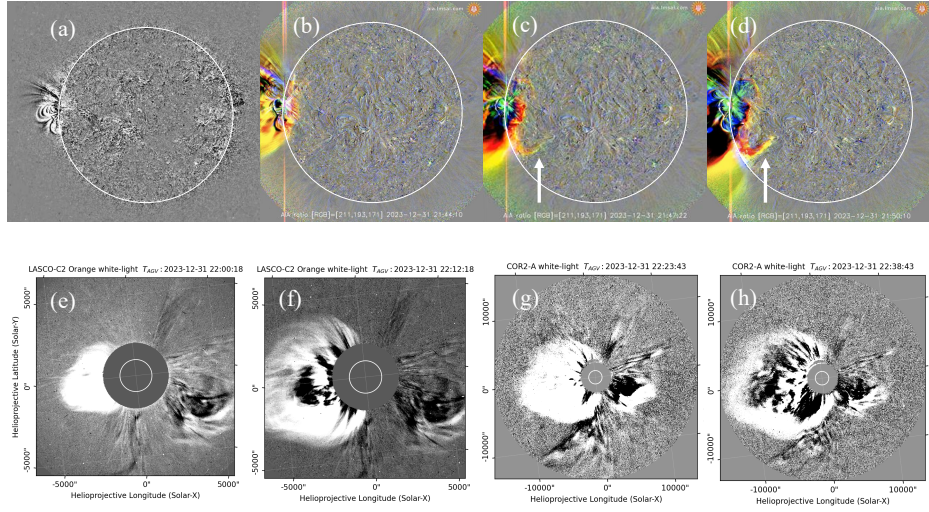


Figure 2. Selection of running-difference images from STA/EUVI at 195 Å (a), SDO/AIA at [211,193,171] Å (b-d), LASCO C2 (e,f), and STA/COR2 (g-h) at different times: 21:42 UT, 21:44 UT; 21:47 UT, 21:50 UT, 22:00 UT, 22:12 UT, 22:24 UT and 22:39 UT. The edge of the solar disk is delimited by white circle in each panel.

a) AIA (panels *b-d*), LASCO-C2, (panels *d-e*), and STA/COR2 (panels *f-g*) observations is presented in Figure 2. The leading edge of the CME crossed the entire field of view of STA/COR2 in less than one hour, making the projected velocity larger than 2400 km/s. According to the SOHO/LASCO CME online catalog¹ (Yashiro et al. 2004; Gopalswamy et al. 2024) the plane-of-sky linear speed of the CME was 2852 km/s. According to the full LASCO catalog, it was among five of the fastest CMEs ever recorded by the instrument since 1996 and the fastest of Solar Cycle 25 (at least until April 2025)². One particular feature that we will focus on is visible in panels *c,d* of Figure 2: a bright loop ahead of the expanding wave, located by a white arrow. It is seen to connect upstream of south-western flank of the expanding wave closer to the center of the solar disk between 21:47 UT and 21:53 UT in SDO/AIA and STA/EUVI images, before being fully engulfed by the expanding coronal wave.

The eruption was also rich in radio emissions. In Figure 3 we present dynamic radio spectra observed by three spacecraft: PSP (at a heliocentric distance of 0.17 AU), STA, and Wind. Measurements by PSP/FIELDS (Bale et al. 2016), STA/WAVES (Bougeret et al. 2008), and Wind/WAVES (Bougeret et al. 1995) are presented in Figure 3 from top to bottom panels, respectively. The frequency of each spectrum is 0.15 MHz to 15 MHz and the time window four hours from 20:00 UT on 2023-12-31 to 00:00 UT on 2024-01-01. The event started at 21:36 UT with a type III burst recorded by PSP/FIELDS. First type III burst at

¹https://cdaw.gsfc.nasa.gov/CME_list/

²Of course, this does not take into account the events that were hidden to LASCO and/or propagating closely to Sun-Earth direction.

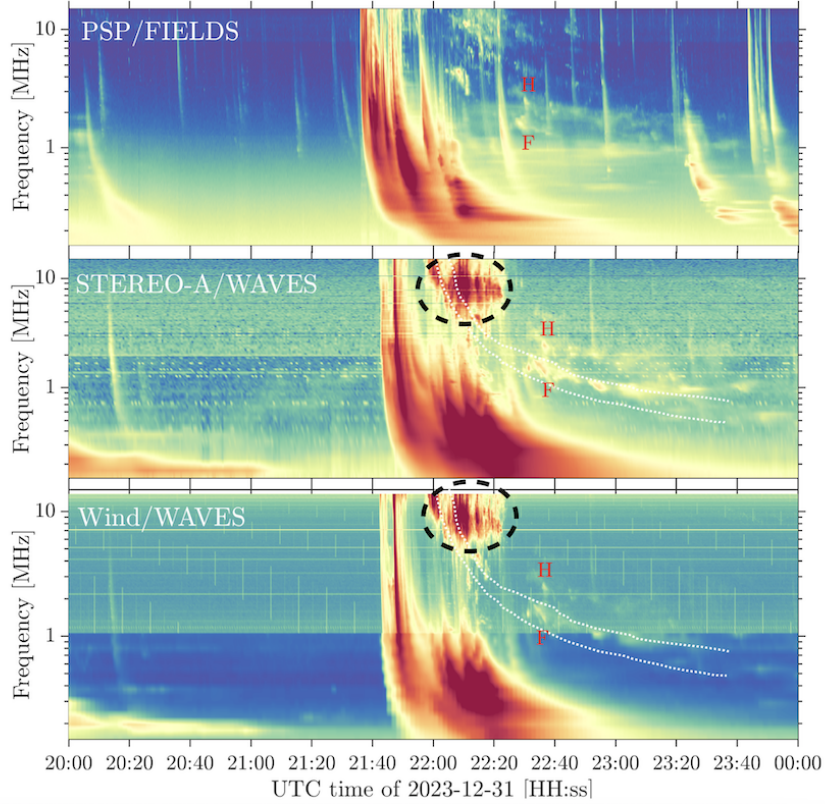


Figure 3. Dynamic radio spectrum observed by PSP/FIELDS (top panel), STEREO-A/WAVES (middle panel) and Wind/WAVES (bottom panel) instruments from 20:00 UT to 00:00 UT on 31 December 2024, in spacecraft time (no shift applied for Light Travel Time differences). The labels ‘F’ and ‘H’ refer to what appear to be fundamental and harmonic emission, respectively. Two white dotted lines are from the shock reconstruction and modeling presented in [Figure 7](#) and described in detail in [section 4](#).

STA and Wind was recorded several minutes later, at 21:42 UT at the highest instrument frequency of 15 MHz. All type III bursts show characteristic fast drifting pattern from 15 MHz to 0.2 MHz. Several other type IIIIs occurred at each observatory up to 22:15 UT, indicating episodes of accelerated electron beams escaping into the the interplanetary medium. The sequence of bursts was clearly different at PSP as compared to Wind and STA. This is logical as PSP was closer to the Sun than both STA and Wind and well-separated in longitude as it was nearly antipodal to L1. The delay in first type III burst onset can be accounted for by light travel time difference from source to the spacecraft of roughly 7 min. The most prominent type III burst at STA and Wind was the second of the series, starting at 21:46:30 UT.

At least one type II burst was observed by each observatory. It started at nearly 21:58 UT at 15 MHz at STA and Wind, and slightly later at PSP. Slowly drifting emission is seen until the end of displayed observations at 00:00 UT on 2024-01-01. It has characteristic patchy features and well-identifiable second

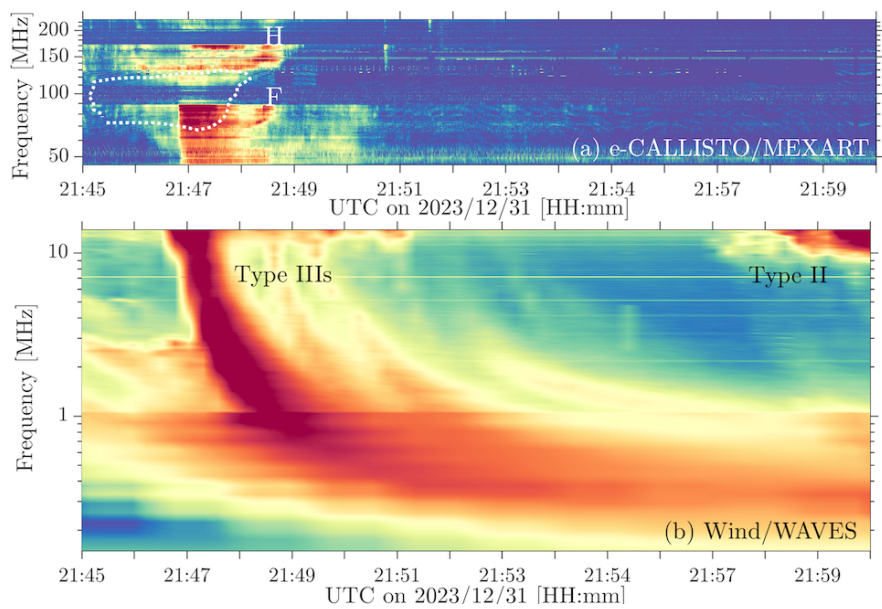


Figure 4. Composite dynamic radio spectrum on 31 December 2023 at frequencies 0.15 - 230 MHz. It consists of spectra from e-CALLISTO MEXART (upper panel) and Wind/WAVES (bottom), from 21:45 UT to 22:00 UT. The labels ‘F’ and ‘H’ refer to what appear to be fundamental and harmonic emission, respectively. The region delimited by white dotted line is the “hotspot” from the shock reconstruction and modeling, described in detail in section 4.

harmonic emission. We performed a linear fit using the frequency drift rate and assuming either Mann (Mann et al. 2023) or Leblanc (Leblanc, Dulk, and Bougeret 1998) coronal density model. According to the fit, the linear radial propagation velocity of emitter was 2000 ± 300 km/s (Mann model) or 1200 ± 200 km/s (Leblanc model) at Wind and STA. Slightly slower velocity was obtained for type II event at PSP/FIELDS.

A patch of intense emission was observed by STA and Wind from 22:00 UT to 22:20 UT in frequency band between 5 MHz and 15 MHz. The corresponding zone is highlighted in middle and lower panels of Figure 3 using black dashed circles. The emission was less intense in PSP/FIELDS observations. It appears as a structured type II burst with “herring bone” features that are frequently observed in intense bursts (Cane and White 1989). The fine-structure of individual pulses can be better captured by large ground based observatories when involved emission occurs at slightly higher frequencies (as shown in Morosan et al. 2019, 2024; Magdalenić et al. 2020; Koval et al. 2023; Jebara et al. 2023a, for recent studies).

Additionally to spacecraft measurements, an interesting radio burst was observed by several ground-based e-CALLISTO radio observatories at > 40 MHz frequencies, including Alaska-HAARP, Australia-ASSA, MEXART (Benz et al. 2009; Monstein, Csillaghy, and Benz 2023)³. In Figure 4 we present a compos-

³<http://www.e-callisto.org/>

ite radio spectrum from e-CALLISTO/MEXART (top panel) at 40-230 MHz frequency range and from Wind/Waves (bottom panel). The time window is smaller than [Figure 3](#) ranging from 21:45 UT to 22:00 UT, allowing to better resolve the high-frequency feature observed by MEXART between 21:47 UT and 21:50 UT. This feature consists of an initial patch between 21:47 UT and 21:48 UT covering all frequencies between 40 MHz to 80 MHz. Then a narrow-band reverse (i.e. towards higher frequencies) drifting feature is observed from 70 MHz at 21:48 UT to 85 MHz at 21:49 UT. A harmonic emission is also clearly drifting from \approx 130 MHz to \approx 160 MHz. The emission weakens after 21:49 UT and disappears after 21:50 UT. We also attempted to fit the radio feature using the Mann and Newkirk coronal density models. The fit provided a radially downward-propagating emitter with 900 ± 200 km/s for both models.

The initial patch is nearly co-temporal with the lower frequency onset of the type III burst measured by Wind/Waves (emissions at 21:47 UT in [Figure 4](#)). This might be a temporal coincidence of two different regions of radio emitting electron distributions, as well as same region producing both. The onset of DH type II burst occurs later, around 21:58 UT as shown in [Figure 4](#) (bottom panel).

High-energy gamma-ray emissions: Fermi-LAT detected > 100 MeV gamma-ray emission of solar origin starting around 22:10 UT and up to 00:23 UT the following day⁴, witnessing the highly energetic nature of this eruption. This CME was therefore able to accelerate protons with energies greater than 300 MeV several hours after the peak of the X-ray flare. Being of nearly two hour duration puts this event at the limit of late-phase (or long-duration) gamma-ray event, as defined by Share et al. (2018). An important note, however, is that the initial phase of the event was uncovered by Fermi-LAT. Thus making timing association of gamma-ray emissions with flare or early shock evolution inaccessible. As in other recent events (e.g., Gopalswamy et al. 2025) we found that the duration of the type II radio burst and of the LAT-detected gamma-ray emission were nearly the same, consistent with the findings of Gopalswamy et al. (2018). Combining Fermi-LAT observations with other observations into a tangible model of particle acceleration is a complex task (e.g., Ackermann et al. 2017; Plotnikov, Rouillard, and Share 2017; Share et al. 2018; Grechnev et al. 2018; Jin et al. 2018; Gopalswamy et al. 2020; Kouloumvakos et al. 2020; Kocharov et al. 2021; Pesce-Rollins et al. 2022, 2024; Bruno et al. 2025), which is not attempted in the present study as our focus is on EUV and radio observations.

Solar energetic particle measurements in-situ: A solar energetic particle (SEP) event was observed by instruments onboard spacecrafts that were largely separated in longitudes (L1, STA, Solar Orbiter, Bepi Colombo, PSP, Mars). The SEP event and onset linked to our eruption was very clear at PSP, Bepi Colombo⁵ and in martian environment as measured by MAVEN and TGO-Liulin (Semkova et al. 2025). Magnetic connection was poor for L1, STA and Solar Orbiter in addition to high pre-event fluxes at their locations because of SEP event originating from earlier eruption on the western side of the Sun. A dedicated

⁴According to Fermi Solar Flare Observations facility available at https://hesperia.gsfc.nasa.gov/fermi_solar/

⁵Marco Pinto, private communication

study relating the shock and SEP properties from this event will be done in a separate work.

3. Shock reconstruction

In order to reconstruct the three-dimensional (3D) kinematic properties of the coronal shock we follow the method developed by Rouillard et al. (2016) and improved in a series of following studies (e.g., Kouloumvakos et al. 2019, 2022a; Jarry et al. 2024). It relies on the ellipsoid model of the expanding coronal pressure wave (Kwon, Zhang, and Olmedo 2014) and on established techniques of shock identification in EUV and white-light observations (e.g., Vourlidas et al. 2003; Vourlidas and Ontiveros 2009; Rouillard et al. 2012). When available, simultaneous well-separated viewpoint observations are used to constrain the 3D extension of the shock at different times. For this event, we used observations from L1 and STEREO-A viewpoints during early expansion (before 22:15 UT), using data from SDO/AIA, SOHO/LASCO coronagraphs, STA/EUVI and STA/COR2.

This type of analysis was made more challenging by the fact that Earth and STA were separated by 7 degrees in longitude. Both had lateral view of the CME expansion from nearly the same perspective. Later expansion (after 22:20 UT) was also observed by PSP/WISPR (Vourlidas et al. 2016) when the apex of the structure was far enough to be seen in Heliospheric Imagers. By the time of the event, PSP was located nearly on the opposite side of the Sun (193 degrees longitudinal separation with Earth) at radial distance of 0.17AU or $36.5R_{\odot}$. It provided a valuable viewpoint to constrain the global shape of the evolved structure, as it had nearly a lateral view from the opposite side. For its later evolution (after 23:30 UT; not reported here) we also used STA/HI1 and SOLO/HI observations to check that the self-similar evolution from earlier fittings was consistent with late-time expansion into the inner heliosphere. The analysis was performed using *PyThea* shock wave analysis software⁶ (Kouloumvakos et al. 2022a) from 21:42 UT to 23:30 UT.

In Figure 5, we present an overview of the shock reconstruction results. Panels *a-d* show the running-difference images of STA/EUVI at 21:45 UT, LASCO/C2 at 22:15 UT, STA/COR2 and PSP/WISPR at 22:53 UT, respectively. The best fit of the shock is over-plotted using a red mesh. In panel *e*, we show the time-evolution of heights of the structure at the sequence of reconstructed times and in panel *f* the derived time-evolution of the corresponding velocities. During the early evolution, we assumed that the shape of the structure was close to a spheroid, that is statistically a reasonable approximation (Jarry et al. 2023). Thus, constraining the lateral expansion of the structure from observations provided a reasonable estimate of the ellipsoid size in the line-of-sight direction. Later on, when PSP/WISPR observation could be used, the structure appeared

⁶www.pythea.org

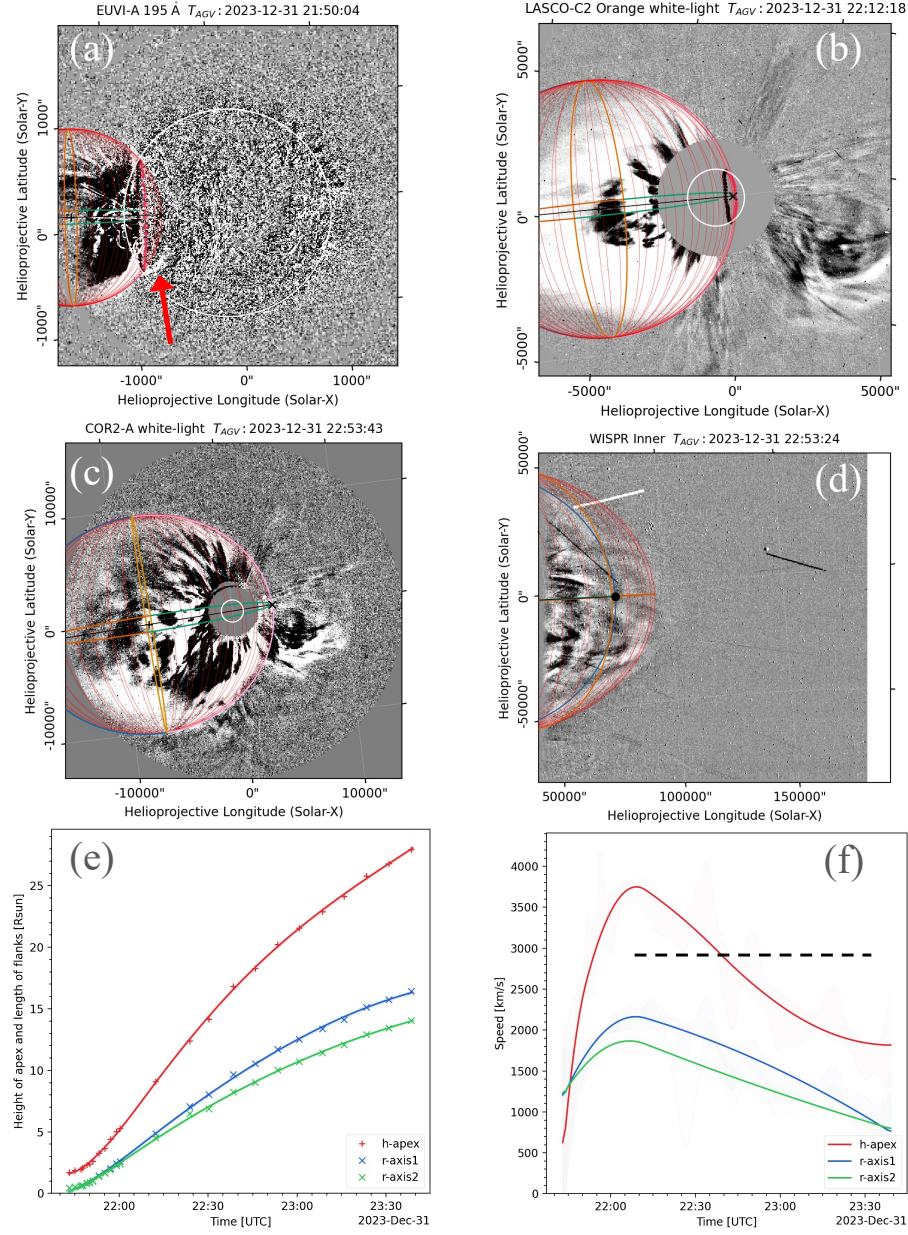


Figure 5. Results of the coronal shock reconstruction. Panel a: STA/EUV running-difference image at 21:50 UT with the fitted shock surface shown using red-colored mesh. Panel b: same but for LASCO-C2 image at 22:12 UT. The red arrow indicates the location of the blighted loop ahead of the shock front. Panels c-d: reconstructed shock on STA/COR2 and PSP/WISPR-IN images at 22:53 UT. Panel c: heights of the apex and ortho-radial axes of the fitted shock at all times used for reconstruction. Panel f: derived speeds. Dashed horizontal line shows the linear speed value from SOHO/LASCO CME catalogue discussed in section 2.

to gradually evolve into slightly oblate ellipsoid (see difference between blue and green lines in panels *c* and *d*).

It appears that the shock had rapid expansion into the solar corona exceeding shortly 3500 km/s around 22:10 UT and then decelerating. The average transit speed through the corona is consistent with the value given by the LASCO catalogue, indicated in [Figure 5\(d\)](#) by the horizontal dashed line (2852 km/s, see quote in [section 2](#)).

In the following step, we combined the expansion of the shock with a background MHD model of the corona. As in previous studies (Rouillard et al. 2016; Plotnikov, Rouillard, and Share 2017; Kouloumvakos et al. 2019, 2022b; Jarry et al. 2024), we used publicly available simulation provided by Predictive Science Inc. (Lionello, Linker, and Mikić 2009; Riley et al. 2011) employing the Magnetohydrodynamic Algorithm outside A Sphere Thermodynamic (MAST) code. It is a 3D MHD model that uses SDO/HMI magnetograms as inner boundary input of the magnetic field and employs advanced thermodynamics for coronal conduction and parametrized coronal heating. It was proven to accurately reproduce coronal plasma and magnetic field conditions in the corona (Lionello, Linker, and Mikić 2009; Riley et al. 2011)⁷. The result of this combination enables the derivation of various parameters of the shock, such as Mach numbers, compression ratio, shock-normal obliquity with respect to the upstream magnetic field direction as well as tracing magnetic connectivity inside solar corona at radial distances extending from solar surface to $30R_{\odot}$. We did not apply any rescaling factors to magnetic field intensity or density provided by the simulation output. The influence of this choice will be discussed in [section 5](#).

4. Results

In [Figure 6](#), we present the distribution of different quantities on the reconstructed shock surface at 21:47 UT as seen from Earth point-of-view. Panels *a-d* show the fast magneto sonic Mach number M_{fm} , Alfvén Mach number M_A , shock front speed V_{sh} , and shock obliquity angle θ_{Bn} distributions, respectively. The solar surface is mapped with EUV image from SDO/AIA at 193 Å wavelength.

For this early time during the eruption, the shock apex was already fast (exceeding 1600 km/s), but most of the surface of the pressure wave was not yet forming a strong shock ($M_{fm} < 2$), except a clearly visible region at the southwestern flank where $M_{fm} > 6$, $M_A > 20$, $V_{sh} \approx 950$ km/s, and $\theta_{Bn} \approx 80^\circ - 90^\circ$. More detailed inspection of the magnetic configuration of this region showed that it corresponds to the cusp of a pseudo-streamer region where the magnetic field strength drops significantly, favoring locally the formation of a strong shock (speed exceeding local $V_A \simeq 100$ km/s). This shock region was quasi-perpendicular, favoring rapid electron acceleration by SDA mechanism (Mann et al. 2018; Wu et al. 2021; Amano et al. 2022). Such a configuration lasted for

⁷https://www.predsci.com/mhdweb/data_access.php

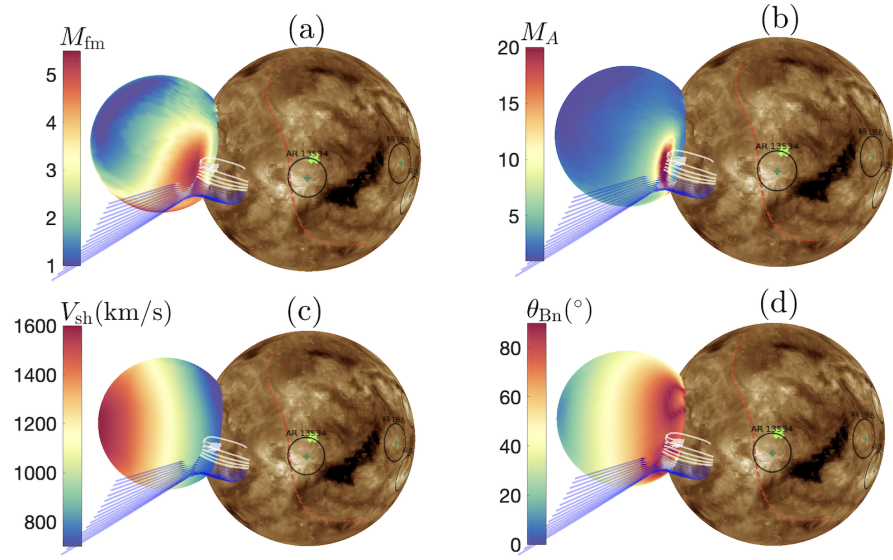


Figure 6. Fitted shock surface on 2023-12-31 at 21:47 UT as seen from Earth position. The color-coding shows the distribution of fast-magneto-sonic Mach number M_{fm} (panel a), Alfvén Mach number M_A (panel b), shock front speed (panel c), and the angle between shock-normal and the upstream magnetic field vector θ_{Bn} (panel d). Solar surface is mapped with 193 Å EUV image recorded by SDO/AIA. A selection of field lines crossing the high M_{fm} and M_A regions is plotted using blue and white lines corresponding to open and closed field lines, respectively. Red dotted line across solar surface delimits the magnetic field inversion line (HCS). Sub-Earth radial projection point is indicated by a green 'x' symbol and NOAA active regions are located by black circles with dark green cross in the center.

nearly 3 minutes until the wave crossed low magnetic field region and became low-Mach number again (but not yet fully engulfing the foot-point positions of the blue lines). Magnetic connectivity lines from this “hotspot” are shown by blue (open) and white (closed) lines in Figure 6. The Sun-directed part of the blue lines follow visually the shape of the flux-tube seen in EUV, see Figure 2 (panels c and d). The other end recrosses the shock at larger radii and connects to outer corona nearly radially. The EUV map also confirms the open-field nature as it shows a dim region where the blue lines connect, indicating a coronal hole region. The field-line tracing from the hotspot shock locations was also performed using independent PFSS field configuration, resulting in sensitively similar field topology to the MAST simulation. These lines are not shown in Figure 6 as they nearly overlap with MAST field lines. By 21:52 UT the shock fully covered the region of interest.

According to Kouloumvakos et al. (2021) the Alfvén Mach number is a convenient indicator of which regions of the shock surface are most efficient at producing type II radio emissions in conjunction with a favorable shock geometry from oblique to quasi-perpendicular. Our procedure following the same approach as in Kouloumvakos et al. (2021) and Jebaraj et al. (2021). This method projects each part of the shock onto frequency- M_A space and then selects the

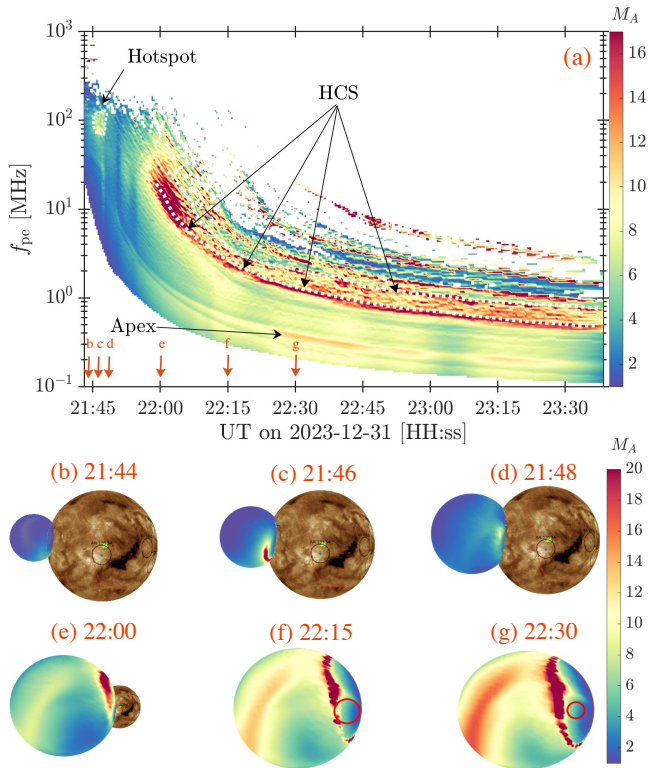


Figure 7. Synthetic radio spectrum based on shock M_A values (panel a). Bottom panels (b-g): snapshots of M_A distribution on fitted shock surface, as seen from Earth viewpoint, at different selected times (indicated by red arrows in upper panel). In two last sub-panels at 22:15 UT (f) and 22:30 UT (g) the position of solar disc (hidden under the expanding shock) is shown by a red circle. Two dotted white lines follow the evolution of low- and intermediate-frequencies regions of shock-HCS interaction (dark red zones corresponding to $M_A > 14$). These two lines are reported in Figure 3 on top of STA/Waves and Wind/Waves spectra. The region around the bright region at the upper left corner, labeled as “hotspot”, is encircled using white dotted line. It is reported into Figure 4, upper panel.

mean value of M_A for each frequency⁸. The frequency is assumed to be the local electron plasma frequency extracted from MAST MHD coronal simulation, $f_{pe} = 8.98\sqrt{N_e/1\text{cm}^{-3}}$ kHz. Performing this at multiple time-steps provides the shock-mediated dynamic spectrum.

In Figure 7 we show the synthetic radio spectrum (upper part, panel a) that maps M_A value of different regions of the shock into time-frequency map according to the procedure described above. The lower part (panels b-g) shows the distribution of M_A on the shock surface at six selected times: 21:44, 21:46, 21:48, 22:00, 22:15, and 22:30 UT. The solar surface is presented with 193 Å map in each panel (as in Figure 6). It appears that the hotspot of nearly 3 min duration (21:45 UT to 21:48 UT) was located on the lower Western part of the

⁸In the original method of Kouloumvakos et al. (2021) they selected the median value.

expanding shock. Later evolution shows that high- M_A regions correspond to the interaction of the shock with the HCS. The position of the HCS can be readily intuited by inspecting the orientation of the red dashed line on solar surface in [Figure 6](#) (magnetic inversion line that evolves at large radii into coronal streamer and the HCS). Hence, different dark red lines in panel a correspond to different emission regions of the shock interaction with the HCS. We also notice that the region around the shock nose (i.e., labeled as ‘Apex’ in the figure) appears as weaker emitter. Indeed, despite having high speed this region has lower M_A than HCS-interacting flanks, propagates through lower density regions, and has more quasi-parallel geometry disfavoring fast electron acceleration by shock. All these factors might contribute to the non-appearance of apex regions in the observed dynamic radio spectrum.

The synthetic spectrum can be used to directly compare our modeling with observations. Two white dotted lines in [Figure 7a](#)) follow two defined high- M_A regions that correspond to regions of shock interaction with the HCS. These two lines are reported in [Figure 3\(b,c\)](#) where STA/Waves and Wind/Waves radio observations are shown. It appears that the observed type II burst signatures are located in between these two lines, slightly closer to the upper (intermediate frequency shock-HCS interaction line). The hotspot related region is encircled by white-dotted line in upper left corner and is reported in [Figure 4\(a\)](#) that shows MEXART observations. We note that the modeled region starts roughly 1 min earlier than the bulk of observed radio emission. However, the bandwidth and duration of the emission is reasonably consistent with modeled hotspot region.

4.1. Input from fast shock acceleration theory of electrons

The Mach number of the shock is not the only relevant quantity that tracks radio-producing regions at the shock. According to established theory of type II radio bursts, the emission occurs from interaction of shock-accelerated electron beams and local upstream plasma (e.g. Mann and Klassen [2005](#)). The shock has to be locally highly oblique and fast in order to form fast enough electron beams near the front, driving local Langmuir wave growth. According to Mann et al. ([2018](#)), the pre-condition triggering the instability reads as $V_b/(\sqrt{3}V_{th,e}) > 1$. Where $V_b = V_{sh}(1 + \cos \alpha_{lc})/\cos \theta_{Bn}$ is the speed of the beam, $V_{th,e}$ is the local coronal electron thermal speed, and the loss-cone angle is related to the overshoot value of magnetic field at the shock front as $\alpha_{lc} = \arcsin \sqrt{B_1/B_{ov}}$. The produced turbulence of Langmuir waves is then partly converted into electromagnetic emission at local plasma frequency and/or its harmonics. Adopting the theoretical formalism of Mann et al. ([2018, 2022](#)), we diagnose which regions of the expanding coronal shock are able to trigger the instability with high enough number density of accelerated electrons to power radio emissions. For this purpose, we used three derived quantities considered as representatives of shock-acceleration efficiency of electrons and emission intensity in radio waves:

- i) Instability criterion: $L_c = V_b/(\sqrt{3}V_{th,e})$. As mentioned earlier, this quantity has to be larger than 1 in order to produce the beam-driven instability driving Langmuir waves. Mapping of L_c on the whole surface of the shock was

firstly done by Kouloumvakos et al. (2021) in the study of 05 November 2014 eruption.

- ii) Fraction of electrons that is accelerated by reflection on the shock front N_{acc}/N_1 , derived according to Equation (32) in Mann et al. (2022). The shock reconstruction coupled with MHD coronal model provides all necessary information for this calculation, assuming upstream electron temperature is equal to proton temperature, $T_e = T_p = T_1$.
- iii) Efficiency of conversion of beam kinetic energy into radio waves, defined as $\varepsilon_{\text{rad}} = QW_b/W_{\text{radio}}$. This parameter combines the previous two, as the kinetic energy density of the beam is $W_b = 0.5N_{\text{acc}}m_eV_b^2$. Here, we adopted the conversion factor $Q = 10^{-6}$ which is a conservative value. It is three times smaller than derived in original study of Ginzburg and Zhelezniakov (1958) as recent fully-kinetic simulations indicate that only a small fraction of produced transverse waves is escaping as O-mode and X-mode emission (Krafft et al. 2025), while larger fraction is contained near the source in form of Z-mode waves. Yet, conversion efficiencies are always higher than $Q = 10^{-6}$ (see Figure 2 in Krafft et al. 2025). Following Mann et al. (2022) (Equation 34), when estimating W_{radio} we assumed that the type II burst observed at 1 AU has a typical flux of 10^3 sfu and then rescaled the radio emissivity down to the Sun (or emission distance of the shock when it is far from the Sun). The bandwidth of $\Delta f = 10$ MHz was assumed, typical for type II bursts.

These three quantities were estimated over the reconstructed evolution of the shock surface and casted into the synthetic spectrum, following the same method as for M_A in Figure 7 (panel a). We present the result of this analysis in Figure 8. The L_c , N_{acc}/N_1 , and ε_{rad} parameters are presented in separate panels from top to bottom, respectively. The left side panels *a-c* employed the loss-cone angle α_{lc} with magnetic ratio $B_{\text{ov}}/B_1 = B_2/B_1 = X_M$ as in Mann et al. (2018, 2022) studies and the right-side panels used the theoretical expression of Gedalin (2021) further applied and fitted to *in-situ* data of shock crossings by Lindberg et al. (2025) : $B_{\text{ov}}/B_1 = \sqrt{0.14M_A^2 + 2.9}$. In the bottom panels *c* and *f* we also over-plotted the locations of the hotspot and DH type II burst observed by Wind/Waves (from analysis of Figures 2 and 3) using greed dotted line and green squares, respectively.

Regions with $L_c < 1$ were excluded in all panels of Figure 8, in order to see only the instability-triggering parts of the shock. As can be seen in all panels, only few regions of the shock surface are able to produce fast enough electron beam. Late in the evolution, after 22:20 UT, these regions are particularly rare as the shock becomes mostly quasi-parallel except inside the interaction parts with the HCS⁹. By comparing two top panels *a* and *d*, we remark that L_c value appears to be weakly sensitive to the choice of B_{ov}/B_1 (i.e. value of α_{lc}). It is expected as $\cos \alpha_{\text{lc}}$ factor changes only slightly the value of L_c .

⁹We also explicitly tested the importance of quasi-perpendicular shocks by excluding all $\theta_{Bn} < 70^\circ$ regions. It resulted in total disappearance of $L_c > 1$ regions in all cases. Thus confirming that only the shock parts with $\theta_{Bn} > 70^\circ$ are sourcing sufficiently fast beams that lead to radio emission.

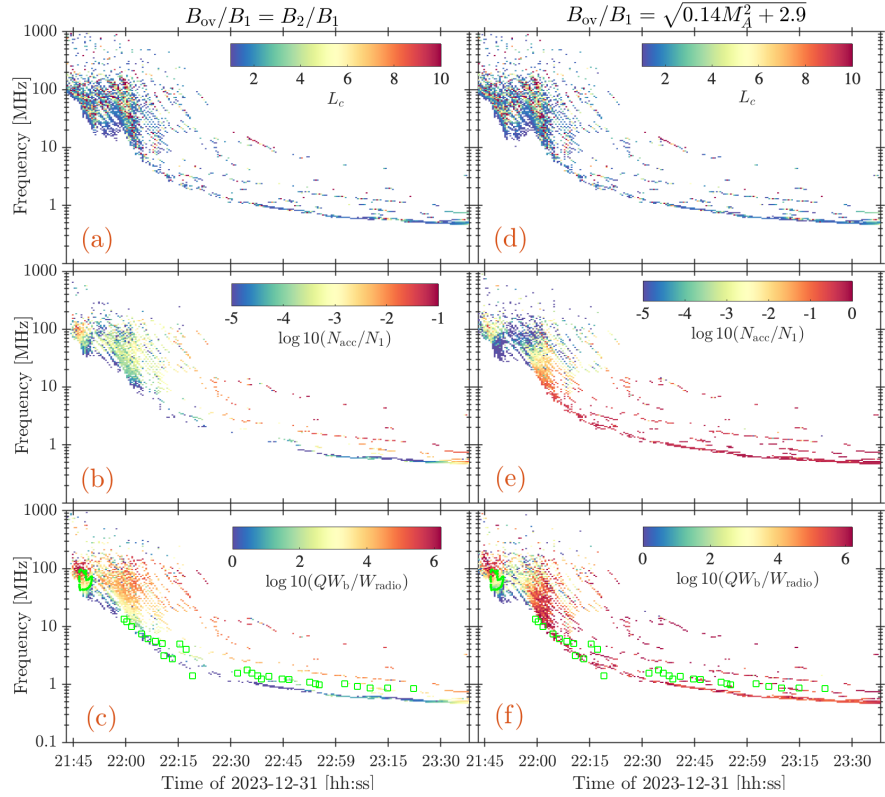


Figure 8. Same as Figure 7(panel a), here presenting the instability criterion L_c (panels a and d), accelerated electron fraction N_{acc}/N_1 (panels b and e), and efficiency of conversion of beam kinetic energy into radio waves ε_{rad} (panels c and f). Regions where instability is not triggered, i.e. $L_c < 1$, were excluded in all panels. The left side panels a-c employed the loss-cone angle α_{lc} value with magnetic overshoot ratio $B_{ov}/B_1 = B_2/B_1 = X_M$ and the right-side panels used: $B_{ov}/B_1 = \sqrt{0.14M_A^2 + 2.9}$. In the bottom panels c and f the locations of the “hotspot” and DH type II burst signatures observed by Wind/Waves (from analysis of Figure 3 and Figure 4) using green dotted line and green squares, respectively.

The picture is very different for N_{acc}/N_1 (panel b vs panel e). For the choice of $B_{ov}/B_1 = B_2/B_1$ (panel b) as typically done in Mann et al works, the values of N_{acc}/N_1 evolve in range between 10^{-6} and 0.1. While for $B_{ov}/B_1 = \sqrt{0.14M_A^2 + 2.9}$, the values are similar to the former before 21:55 UT but become nearly equal to 1 after $\sim 22:00$ UT. Thus, implying that all incoming electrons are reflected at the shock front which is highly questionable physically.

Finally, the radio emissivity parameter ε_{rad} is presented in panels c and f. It is expected to directly compare with observations. The emissivity is very high early on in both cases, but drops significantly after 21:50 UT in panel c, while remaining very high in panel f. Some tiny regions of the shock surface appear to be able to generate $\varepsilon_{rad} > 10^4$ inside the intermediate and upper shock-HCS interaction regions, while the lower main shock-HCS line has $\varepsilon_{rad} \sim 1 - 10$. In

the case of $B_{\text{ov}}/B_1 = \sqrt{0.14M_A^2 + 2.9}$ (panel f) all regions have $\varepsilon_{\text{rad}} > 10^5$ since they mostly correspond to high- M_A and $N_{\text{acc}}/N_1 \simeq 1$ regions.

For visual comparison, we over plotted in bottom panels the “hotspot” region from [Figure 4](#)(panel *a*) using green dotted line and DH type II signatures using green square symbols, extracted from Wind/Waves observations in [Figure 3](#). Early evolution compares well with ε_{rad} distribution. The “hotspot” region between 21:44 UT and 21:47 UT is nearly in overlap with observed region, in green. Yet, the most intense modeled emission occurs slightly earlier and at slightly higher frequencies than observed. Between 22:00 UT and 22:15 UT the overlap between synthetic and observed emission regions is particularly good, i.e. when shock-HCS interaction emerges (see panels *e* and *f* in [Figure 7](#)). After 22:30 UT it appears that the intermediate shock-HCS interaction line matches better observed type II signatures despite being more intermittent but emitting at higher values of ε_{rad} than the main shock-HCS line that evolves at slightly lower frequencies with regular pattern.

5. Discussion and conclusion

The results of our work inferred efficient acceleration of energetic electrons by the transient high-Mach quasi-perpendicular shock in the low corona. By examining EUV observations we focused on a particular feature ahead of the shock wave between 21:47 UT and 21:53 UT (see [Figure 2](#) upper row), resembling an illuminated flux tube. By examining radio observations there was radio emission between 21:46 UT and 21:49 UT in 40 MHz to 140 MHz frequency range with reverse drifting features (as shown in [Figure 4](#)). By reconstructing the shock front evolution ([section 3](#)) we then found in [section 4](#) that the EUV flux tube feature and radio emission can both be attributed to the transient high- M_A quasi-perpendicular shock patch on the Earth-sided flank of the coronal pressure wave. We then demonstrated in [subsection 4.1](#) that this region was highly efficient at accelerating electrons by SDA with enough energy density to power radio emission. The same analysis presented [Figure 8](#) of late evolution indicated good agreement between regions able to drive electron beam instability at shock, i.e. $L_c > 1$, and drifting DH type II burst.

There are, however, some discrepancies between our modeling and observations. Firstly, reconstructed field lines that connect the hotspot to the solar surface are similar but do not follow exactly the apparent topology of EUV flux tube. Modeled lines are few degrees closer to the solar equator. These lines are open field lines in agreement with 193 Å EUV maps where shaded regions were seen to be illuminated. An important test of electron acceleration efficiency by this shock region would have been possible if direct magnetic connection of a spacecraft to this region occurred (as done in, e.g., Morosan et al. 2024, for a different event). Unfortunately, it did not happen as the spacecraft fleet was not positioned favorably. All available probes were connected far away. Secondly, there was about one minute difference between modeled and observed radio emission by MEXART, as seen in [Figure 4\(a\)](#).

Despite these differences, it is remarkable that the plasma emission from the shock-hotspot region falls into consistent range of frequencies and traced field lines visually resemble observed flux tube in EUV during the correct time range. In some reconstruction results we found that the hotspot was sliding from higher to lower heights with time, potentially explaining the reverse drifting radio emission of one minute duration between 21:48 UT and 21:49 UT. The difference in onset time and field line topology discrepancy could be due to two main reasons: (i) shock fitting did not capture properly the shock position at relevant time and (ii) MAST simulation did not capture the position and orientation of the pseudo-streamer with required accuracy. For the former, we tried several strategies of shock fittings. In some cases largely exaggerating the expansion speed and main direction of propagation. None on these tries was successful in reproducing both the onset time and frequency range of hotspot-related emissions. We hence favor the latter explanation since even a slight shift (few degrees) of pseudo-streamer position could account for one minute delay between modeling and observation. We also expect that a slight southward shift of the pseudo-streamer's cusp would improve agreement between hotspot-connected field lines and EUV-brightened flux tube.

We did not apply any correction factor on magnetic field intensity and plasma density from MAST MHD simulations. Indeed, it was common in previous studies to apply some correction factor (constant in the whole box), based on comparison between open magnetic flux in the simulation and field intensity measured in-situ (Rouillard et al. 2016; Kouloumvakos et al. 2019, 2021). For densities, correction factors between 0.5 and 3 were applied by Kouloumvakos et al. (2019, 2021); Morosan et al. (2024). Despite observational motivations (Wang et al. 2017), we did not follow this procedure because (1) applying a constant correction factor everywhere in the simulation box will only improve some localized regions and (2) rescaling by hand one physical quantity modifies in principle the pressure balance in non-trivial way. In the present study, we noticed that rescaling densities by a factor of 2 will make the main shock-HCS interaction region correspond nearly perfectly to the observed type II burst pattern by STA and Wind (up-shift of lower dotted white line in Figure 3b,c). But at the same time it will shift the “hotspot”-related emission to too high values as compared to observations. We conclude that methodological improvements are necessary for both shock reconstruction and steady-state coronal MHD simulations if one wants to capture small scale features (but still much larger than kinetic).

In terms of shock physics, we studied which parts of evolving shock surface were efficient at producing energetic electrons and driving radio emissions in subsection 4.1. Two different prescriptions for the value of magnetic overshoot at the shock front were adopted. The most simple assumption that the overshoot value is equal to downstream value ($B_{ov} = B_2$) provided sufficient level of radio emissivity at times and frequencies consistent with those of the observed type II radio bursts. On the other hand, the prescription $B_{ov}/B_1 = \sqrt{aM_A^2 + b}$ (Gedalin 2021) while being motivated theoretically and by in-situ measurements near 1 AU and Saturn's bow shock (Jebaraj et al. 2023b; Lindberg et al. 2025), leads to nonphysically large values of reflected electron densities at the shock when

the Alfvén Mach number is particularly high ($M_A > 10$)¹⁰. The issue with this prescription at large M_A was already noticed by Lindberg et al. (2025), the data indicating flattening of B_{ov}/B_1 instead of rising as $\propto M_A$. Our analysis of a fast shock inside solar corona shows that this prescription has to be revised for $M_A \gg 10$ shocks, especially regarding the requirement to fix the upper bound of B_{ov}/B_1 in this regime.

5.1. Conclusion

To conclude, in the present work we studied several aspects of the coronal shock from the 31st December 2023 eruption. We focused on observational reconstruction of the coronal shock evolution and its role in producing radio emissions. By field line tracing and producing a synthetic radio spectrum we found that the short-lived radio emissions at ~ 100 MHz can be explained by a transient “hotspot” (high Mach number and quasi-perpendicular shock at the cusp of pseudo-streamer) region that also reproduces rarely observed upstream flux tube illumination seen in EUV images. Our methodology was also efficient in reproducing the DH type II burst evolution as shock-HCS interaction regions, consolidating similar conclusion of previous studies (e.g., Cho et al. 2008; Jebaraj et al. 2021; Frassati et al. 2022; Koval et al. 2023). We also note that very similar conclusions were found in recent study of Bhandari, Morosan, and Normo (2025) that used similar methodology to the present work for ten events of Solar Cycle 25. Our methodology merits more general application to other type II bursts and related coronal shock waves in order to assess the general relevance of shock–pseudo-streamer and shock–HCS interaction regions as important places of significant particle acceleration and dominant emitting regions of type II bursts.

Acknowledgements I.P. is grateful to K.L. Klein for insightful discussions and suggestions and **Marco Pinto for providing Bepi Colombo/BERM data (not presented in the main text)**. I.P. acknowledges the European Union’s Horizon-2020 research and innovation program for support under grant agreement No. 101004159 (SERPENTINE). This article reflects only the authors’ view and the European Commission is not responsible for any use that may be made of the information it contains. A.K. acknowledges financial support from NASA’s LWS grant 80NSSC25K0130 and HGO grant 80NSSC24K0555. We acknowledge the e-CALLISTO; Wind/WAVES; STEREO; SOHO/LASCO; SDO/AIA; PSP teams and Predictive Science Inc. for providing open data access used in this study. The STEREO/SECCHI data are produced by a consortium of RAL (UK), NRL (USA), LMSAL (USA), GSFC (USA), MPS (Germany), CSL (Belgium), IOTA (France), and IAS (France). SOHO is a mission of international cooperation between ESA and NASA. The SDO/AIA data used are courtesy of SDO (NASA) and the AIA consortium. We acknowledge usage of the tools made available by the French plasma physics data center (Centre de Données de la Physique des Plasmas; CDPP; <http://cdpp.eu/>), CNES and the space weather team of Toulouse at Solar-Terrestrial Observations and Modellings Service (STORMS; <https://stormsweb.irap.omp.eu/>). In particular,

¹⁰We also tried all different values of a and b from (Lindberg et al. 2025) study, obtaining too large $N_{\text{acc}}/N_1 \sim 1$ in all cases.

present study used the Propagation Tool (<http://propagationtool.cdpp.eu>), and the Magnetic Connectivity Tool (<http://connect-tool.irap.omp.eu/>). This research has also made use of PyThea v1.0.0, an open-source and free Python package to reconstruct the 3D structure of CMEs and shockwaves (Kouloumvakos et al. 2022a). The LASCO/CME catalog is generated and maintained at the CDAW Data Center by NASA and The Catholic University of America in cooperation with the Naval Research Laboratory.

Data Availability SDO/AIA data is publicly available at <https://aia.lmsal.com/>. CME and pace-based radio burst data is publicly available at the CDAW Data Center (<https://cdaw.gsfc.nasa.gov>). The ground-based radio data are available at <https://e-callisto.org>. Predictive Science Inc. simulations are publicly available at https://www.predsci.com/mhdweb/data_access.php. Coronal shock reconstructions (table of fits) is available on request to the corresponding author.

References

- Ackermann, M., Allafort, A., Baldini, L., Barbiellini, G., Bastieri, D., Bellazzini, R., Bissaldi, E., Bonino, R., Bottacini, E., Bregeon, J., Bruel, P., Buehler, R., Cameron, R.A., Caragiulo, M., Caraveo, P.A., Cavazzuti, E., Cecchi, C., Charles, E., Ciprini, S., Costanza, F., Cutini, S., D’Ammando, F., de Palma, F., Desiante, R., Digel, S.W., Di Lalla, N., Di Mauro, M., Di Venere, L., Drell, P.S., Favuzzi, C., Fukazawa, Y., Fusco, P., Gargano, F., Giglietto, N., Giordano, F., Giroletti, M., Grenier, I.A., Guillemot, L., Guiriec, S., Jogler, T., Jóhannesson, G., Kashapova, L., Krucker, S., Kuss, M., La Mura, G., Larsson, S., Latronico, L., Li, J., Liu, W., Longo, F., Loparco, F., Lubrano, P., Magill, J.D., Maldera, S., Manfreda, A., Mazziotta, M.N., Mitthumsiri, W., Mizuno, T., Monzani, M.E., Morselli, A., Moskalenko, I.V., Negro, M., Nuss, E., Ohsugi, T., Omodei, N., Orlando, E., Pal’shin, V., Paneque, D., Perkins, J.S., Pesce-Rollins, M., Petrosian, V., Piron, F., Principe, G., Rainò, S., Rando, R., Razzano, M., Reimer, O., Rubio da Costa, F., Sgrò, C., Simone, D., Siskind, E.J., Spada, F., Spandre, G., Spinelli, P., Tajima, H., Thayer, J.B., Torres, D.F., Troja, E., Vianello, G.: 2017, Fermi-LAT Observations of High-energy Behind-the-limb Solar Flares. *Astrophys. J.* **835**, 219. [DOI](#). [ADS](#).
- Amano, T., Matsumoto, Y., Bohdan, A., Kobzar, O., Matsujiyo, S., Oka, M., Niemiec, J., Pohl, M., Hoshino, M.: 2022, Nonthermal electron acceleration at collisionless quasi-perpendicular shocks. *Reviews of Modern Plasma Physics* **6**, 29. [DOI](#). [ADS](#).
- Bale, S.D., Goetz, K., Harvey, P.R., Turin, P., Bonnell, J.W., Dudok de Wit, T., Ergun, R.E., MacDowall, R.J., Pulupa, M., Andre, M., Bolton, M., Bougeret, J.-L., Bowen, T.A., Burgess, D., Cattell, C.A., Chandran, B.D.G., Chaston, C.C., Chen, C.H.K., Choi, M.K., Connerney, J.E., Cranmer, S., Diaz-Aguado, M., Donakowski, W., Drake, J.F., Farrell, W.M., Fergeau, P., Fermin, J., Fischer, J., Fox, N., Glaser, D., Goldstein, M., Gordon, D., Hanson, E., Harris, S.E., Hayes, L.M., Hinze, J.J., Hollweg, J.V., Horbury, T.S., Howard, R.A., Hoxie, V., Jannet, G., Karlsson, M., Kasper, J.C., Kellogg, P.J., Kien, M., Klimchuk, J.A., Krasnoselskikh, V.V., Krucker, S., Lynch, J.J., Maksimovic, M., Malaspina, D.M., Marker, S., Martin, P., Martinez-Oliveros, J., McCauley, J., McComas, D.J., McDonald, T., Meyer-Vernet, N., Moncuquet, M., Monson, S.J., Mozer, F.S., Murphy, S.D., Odom, J., Oliverson, R., Olson, J., Parker, E.N., Pankow, D., Phan, T., Quataert, E., Quinn, T., Ruplin, S.W., Salem, C., Seitz, D., Sheppard, D.A., Siy, A., Stevens, K., Summers, D., Szabo, A., Timofeeva, M., Vaivads, A., Velli, M., Yehle, A., Werthimer, D., Wygant, J.R.: 2016, The FIELDS Instrument Suite for Solar Probe Plus. Measuring the Coronal Plasma and Magnetic Field, Plasma Waves and Turbulence, and Radio Signatures of Solar Transients. *Space Sci. Rev.* **204**, 49. [DOI](#). [ADS](#).
- Benz, A.O., Monstein, C., Meyer, H., Manoharan, P.K., Ramesh, R., Altyntsev, A., Lara, A., Paez, J., Cho, K.-S.: 2009, A World-Wide Net of Solar Radio Spectrometers: e-CALLISTO. *Earth Moon and Planets* **104**, 277. [DOI](#). [ADS](#).
- Bhandari, K., Morosan, D.E., Normo, S.: 2025, Comprehensive study of solar type II radio bursts and the properties of the associated shock waves. *arXiv e-prints*, arXiv:2512.21846. [ADS](#).

- Bougeret, J.-L., Kaiser, M.L., Kellogg, P.J., Manning, R., Goetz, K., Monson, S.J., Monge, N., Friel, L., Meetre, C.A., Perche, C., Sitruk, L., Hoang, S.: 1995, Waves: The Radio and Plasma Wave Investigation on the Wind Spacecraft. *Space Sci. Rev.* **71**, 231. [DOI](#). [ADS](#).
- Bougeret, J.L., Goetz, K., Kaiser, M.L., Bale, S.D., Kellogg, P.J., Maksimovic, M., Monge, N., Monson, S.J., Astier, P.L., Davy, S., Dekkali, M., Hinze, J.J., Manning, R.E., Aguilar-Rodriguez, E., Bonnin, X., Briand, C., Cairns, I.H., Cattell, C.A., Cecconi, B., Eastwood, J., Ergun, R.E., Fainberg, J., Hoang, S., Huttunen, K.E.J., Krucker, S., Lecacheux, A., MacDowall, R.J., Macher, W., Mangeney, A., Meetre, C.A., Moussas, X., Nguyen, Q.N., Oswald, T.H., Pulupa, M., Reiner, M.J., Robinson, P.A., Rucker, H., Salem, C., Santolik, O., Silvis, J.M., Ullrich, R., Zarka, P., Zouganelis, I.: 2008, S/WAVES: The Radio and Plasma Wave Investigation on the STEREO Mission. *Space Sci. Rev.* **136**, 487. [DOI](#). [ADS](#).
- Brueckner, G.E., Howard, R.A., Koomen, M.J., Korendyke, C.M., Michels, D.J., Moses, J.D., Socker, D.G., Dere, K.P., Lamy, P.L., Llebaria, A., Bout, M.V., Schwenn, R., Simnett, G.M., Bedford, D.K., Eyles, C.J.: 1995, The Large Angle Spectroscopic Coronagraph (LASCO). *Sol. Phys.* **162**, 357. [DOI](#). [ADS](#).
- Bruno, A., Pesce-Rollins, M., Dalla, S., Omodei, N., Richardson, I.G., Ryan, J.M.: 2025, The 2024 July 16 Solar Event: A Challenge To The Coronal Mass Ejection Origin Of Long-Duration Gamma-Ray Flares. *arXiv e-prints*, arXiv:2510.26666. [DOI](#). [ADS](#).
- Cane, H.V., White, S.M.: 1989, On the Source Conditions for Herringbone Structure in Type-II Solar Radio Bursts. *Sol. Phys.* **120**, 137. [DOI](#). [ADS](#).
- Cho, K.-S., Bong, S.-C., Kim, Y.-H., Moon, Y.-J., Dryer, M., Shanmugaraju, A., Lee, J., Park, Y.D.: 2008, Low coronal observations of metric type II associated CMEs by MLSO coronameters. *Astron. Astrophys.* **491**, 873. [DOI](#). [ADS](#).
- Frassati, F., Laurenza, M., Bemporad, A., West, M.J., Mancuso, S., Susino, R., Alberti, T., Romano, P.: 2022, Acceleration of Solar Energetic Particles through CME-driven Shock and Streamer Interaction. *Astrophys. J.* **926**, 227. [DOI](#). [ADS](#).
- Gedalin, M.: 2021, Shock Heating of Directly Transmitted Ions. *Astrophys. J.* **912**, 82. [DOI](#). [ADS](#).
- Ginzburg, V.L., Zhelezniakov, V.V.: 1958, On the Possible Mechanisms of Sporadic Solar Radio Emission (Radiation in an Isotropic Plasma). *Soviet Astron.* **2**, 653. [ADS](#).
- Gopalswamy, N., Mäkelä, P., Yashiro, S., Lara, A., Xie, H., Akiyama, S., MacDowall, R.J.: 2018, Interplanetary Type II Radio Bursts from Wind/WAVES and Sustained Gamma-Ray Emission from Fermi/LAT: Evidence for Shock Source. *Astrophys. J. Lett.* **868**, L19. [DOI](#). [ADS](#).
- Gopalswamy, N., Mäkelä, P., Yashiro, S., Akiyama, S., Xie, H., Thakur, N.: 2020, Source of Energetic Protons in the 2014 September 1 Sustained Gamma-ray Emission Event. *Sol. Phys.* **295**, 18. [DOI](#). [ADS](#).
- Gopalswamy, N., Michalek, G., Yashiro, S., Mäkelä, P., Akiyama, S., Xie, H., Vourlidas, A.: 2024, The SOHO LASCO CME Catalog – Version 2. *arXiv e-prints*, arXiv:2407.04165. [DOI](#). [ADS](#).
- Gopalswamy, N., Mäkelä, P., Akiyama, S., Xie, H., Yashiro, S., Bale, S.D., Wimmer-Schweingruber, R.F., Kuehl, P., Krucker, S.: 2025, Multispacecraft Observations of the 2024 September 9 Backside Solar Eruption that Resulted in a Sustained Gamma Ray Emission Event. *arXiv e-prints*, arXiv:2503.23852. [DOI](#). [ADS](#).
- Grechnev, V.V., Kiselev, V.I., Kashapova, L.K., Kochanov, A.A., Zimovets, I.V., Uralov, A.M., Nizamov, B.A., Grigorieva, I.Y., Golovin, D.V., Litvak, M.L., Mitrofanov, I.G., Sanin, A.B.: 2018, Radio, Hard X-Ray, and Gamma-Ray Emissions Associated with a Far-Side Solar Event. *Sol. Phys.* **293**, 133. [DOI](#). [ADS](#).
- Howard, R.A., Moses, J.D., Vourlidas, A., Newmark, J.S., Socker, D.G., Plunkett, S.P., Korendyke, C.M., Cook, J.W., Hurley, A., Davila, J.M., Thompson, W.T., St Cyr, O.C., Mentzell, E., Mehalick, K., Lemen, J.R., Wuelser, J.P., Duncan, D.W., Tarbell, T.D., Wolfson, C.J., Moore, A., Harrison, R.A., Waltham, N.R., Lang, J., Davis, C.J., Eyles, C.J., Mapson-Menard, H., Simnett, G.M., Halain, J.P., Defise, J.M., Mazy, E., Rochus, P., Mercier, R., Ravet, M.F., Delmotte, F., Auchere, F., Delaboudiniere, J.P., Bothmer, V., Deutsch, W., Wang, D., Rich, N., Cooper, S., Stephens, V., Maahs, G., Baugh, R., McMullin, D., Carter, T.: 2008, Sun Earth Connection Coronal and Heliospheric Investigation (SECCHI). *Space Sci. Rev.* **136**, 67. [DOI](#). [ADS](#).
- Jarry, M., Rouillard, A.P., Plotnikov, I., Kouloumvakos, A., Warmuth, A.: 2023, Parametric study of the kinematic evolution of coronal mass ejection shock waves and their relation to flaring activity. *Astron. Astrophys.* **672**, A127. [DOI](#). [ADS](#).

- Jarry, M., Dresing, N., Rouillard, A.P., Plotnikov, I., Vainio, R., Palmroos, C., Kouloumvakos, A., Vuorinen, L.: 2024, The evolution of coronal shock wave properties and their relation with solar energetic particles. *arXiv e-prints*, arXiv:2406.07058. [DOI](#). [ADS](#).
- Jebaraj, I.C., Magdalenić, J., Podladchikova, T., Scolini, C., Pomoell, J., Veronig, A.M., Dissauer, K., Krupar, V., Kilpua, E.K.J., Poedts, S.: 2020, Using radio triangulation to understand the origin of two subsequent type II radio bursts. *Astron. Astrophys.* **639**, A56. [DOI](#). [ADS](#).
- Jebaraj, I.C., Kouloumvakos, A., Magdalenić, J., Rouillard, A.P., Mann, G., Krupar, V., Poedts, S.: 2021, Generation of interplanetary type II radio emission. *Astron. Astrophys.* **654**, A64. [DOI](#). [ADS](#).
- Jebaraj, I.C., Kouloumvakos, A., Dresing, N., Warmuth, A., Wijsen, N., Palmroos, C., Gieseler, J., Marmyleva, A., Vainio, R., Krupar, V., Wiegelmann, T., Magdalenić, J., Schuller, F., Battaglia, A.F., Fedeli, A.: 2023a, Multiple injections of energetic electrons associated with the flare and CME event on 9 October 2021. *Astron. Astrophys.* **675**, A27. [DOI](#). [ADS](#).
- Jebaraj, I.C., Dresing, N., Krasnoselskikh, V., Agapitov, O.V., Gieseler, J., Trott, D., Wijsen, N., Larosa, A., Kouloumvakos, A., Palmroos, C., Dimmock, A., Kolhoff, A., Kühl, P., Fleth, S., Fedeli, A., Valkila, S., Lario, D., Khotyaintsev, Y.V., Vainio, R.: 2023b, Relativistic electron beams accelerated by an interplanetary shock. *Astron. Astrophys.* **680**, L7. [DOI](#). [ADS](#).
- Jin, M., Petrosian, V., Liu, W., Nitta, N.V., Omodei, N., Rubio da Costa, F., Effenberger, F., Li, G., Pesce-Rollins, M., Alafont, A., Manchester, W. IV: 2018, Probing the Puzzle of Behind-the-limb γ -Ray Flares: Data-driven Simulations of Magnetic Connectivity and CME-driven Shock Evolution. *Astrophys. J.* **867**, 122. [DOI](#). [ADS](#).
- Kaiser, M.L., Kucera, T.A., Davila, J.M., St. Cyr, O.C., Guhathakurta, M., Christian, E.: 2008, The STEREO Mission: An Introduction. *Space Sci. Rev.* **136**, 5. [DOI](#). [ADS](#).
- Klein, K.-L.: 2021, Radio astronomical tools for the study of solar energetic particles II. Time-extended acceleration at subrelativistic and relativistic energies. *Frontiers in Astronomy and Space Sciences* **7**, 93. [DOI](#). [ADS](#).
- Klein, K.-L., Krucker, S., Trottet, G., Hoang, S.: 2005, Coronal phenomena at the release of solar energetic electron events. *Astron. Astrophys.* **431**, 1047. [DOI](#). [ADS](#).
- Klein, K.-L., Musset, S., Vilmer, N., Briand, C., Krucker, S., Francesco Battaglia, A., Dresing, N., Palmroos, C., Gary, D.E.: 2022, The relativistic solar particle event on 28 October 2021: Evidence of particle acceleration within and escape from the solar corona. *Astron. Astrophys.* **663**, A173. [DOI](#). [ADS](#).
- Klein, K.-L., Salas Matamoros, C., Hamini, A., Kollhoff, A.: 2024, Non-thermal electrons in an eruptive solar event: Magnetic structure, confinement, and escape into the heliosphere. *Astron. Astrophys.* **690**, A382. [DOI](#). [ADS](#).
- Kocharov, L., Omodei, N., Mishev, A., Pesce-Rollins, M., Longo, F., Yu, S., Gary, D.E., Vainio, R., Usoskin, I.: 2021, Multiple Sources of Solar High-energy Protons. *Astrophys. J.* **915**, 12. [DOI](#). [ADS](#).
- Kouloumvakos, A., Rouillard, A.P., Wu, Y., Vainio, R., Vourlidas, A., Plotnikov, I., Afanasiev, A., Önel, H.: 2019, Connecting the Properties of Coronal Shock Waves with Those of Solar Energetic Particles. *Astrophys. J.* **876**, 80. [DOI](#). [ADS](#).
- Kouloumvakos, A., Rouillard, A.P., Share, G.H., Plotnikov, I., Murphy, R., Papaioannou, A., Wu, Y.: 2020, Evidence for a Coronal Shock Wave Origin for Relativistic Protons Producing Solar Gamma-Rays and Observed by Neutron Monitors at Earth. *Astrophys. J.* **893**, 76. [DOI](#). [ADS](#).
- Kouloumvakos, A., Rouillard, A., Warmuth, A., Magdalenić, J., Jebaraj, I.C., Mann, G., Vainio, R., Monstein, C.: 2021, Coronal Conditions for the Occurrence of Type II Radio Bursts. *Astrophys. J.* **913**, 99. [DOI](#). [ADS](#).
- Kouloumvakos, A., Rodríguez-García, L., Gieseler, J., Price, D.J., Vourlidas, A., Vainio, R.: 2022a, PyThea: An open-source software package to perform 3D reconstruction of coronal mass ejections and shock waves. *Frontiers in Astronomy and Space Sciences* **9**, 974137. [DOI](#). [ADS](#).
- Kouloumvakos, A., Kwon, R.Y., Rodríguez-García, L., Lario, D., Dresing, N., Kilpua, E.K.J., Vainio, R., Török, T., Plotnikov, I., Rouillard, A.P., Downs, C., Linker, J.A., Malandraki, O.E., Pinto, R.F., Riley, P., Allen, R.C.: 2022b, The first widespread solar energetic particle event of solar cycle 25 on 2020 November 29. Shock wave properties and the wide distribution of solar energetic particles. *Astron. Astrophys.* **660**, A84. [DOI](#). [ADS](#).

- Koval, A., Stanislavsky, A., Karlický, M., Wang, B., Yerin, S., Konovalenko, A., Bárta, M.: 2023, Morphology of Solar Type II Bursts Caused by Shock Propagation through Turbulent and Inhomogeneous Coronal Plasma. *Astrophys. J.* **952**, 51. [DOI](#). [ADS](#).
- Krafft, C., Volokitin, A.S., Polanco-Rodríguez, F.J., Savoini, P.: 2025, Radiation efficiency of electromagnetic wave modes from beam-generated solar radio sources. *Nature Astronomy* **9**, 1292. [DOI](#). [ADS](#).
- Kwon, R.-Y., Zhang, J., Olmedo, O.: 2014, New Insights into the Physical Nature of Coronal Mass Ejections and Associated Shock Waves within the Framework of the Three-dimensional Structure. *Astrophys. J.* **794**, 148. [DOI](#). [ADS](#).
- Leblanc, Y., Dulk, G.A., Bougeret, J.-L.: 1998, Tracing the Electron Density from the Corona to 1 au. *Sol. Phys.* **183**, 165. [DOI](#). [ADS](#).
- Lemen, J.R., Title, A.M., Akin, D.J., Boerner, P.F., Chou, C., Drake, J.F., Duncan, D.W., Edwards, C.G., Friedlaender, F.M., Heyman, G.F., Hurlburt, N.E., Katz, N.L., Kushner, G.D., Levay, M., Lindgren, R.W., Mathur, D.P., McFeaters, E.L., Mitchell, S., Rehse, R.A., Schrijver, C.J., Springer, L.A., Stern, R.A., Tarbell, T.D., Wueller, J.-P., Wolfson, C.J., Yanari, C., Bookbinder, J.A., Cheimets, P.N., Caldwell, D., Deluca, E.E., Gates, R., Golub, L., Park, S., Podgorski, W.A., Bush, R.I., Scherrer, P.H., Gummin, M.A., Smith, P., Auker, G., Jerram, P., Pool, P., Soufli, R., Windt, D.L., Beardsley, S., Clapp, M., Lang, J., Waltham, N.: 2012, The Atmospheric Imaging Assembly (AIA) on the Solar Dynamics Observatory (SDO). *Sol. Phys.* **275**, 17. [DOI](#). [ADS](#).
- Lindberg, M., Hietala, H., Shirazul, K., Trotta, D., Sulaiman, A.H., Burkholder, B.L., Dimmock, A.: 2025, Statistical Study of Magnetic Overshoots at Collisionless Shocks. *Journal of Geophysical Research (Space Physics)* **130**, e2024JA033659. [DOI](#). [ADS](#).
- Lionello, R., Linker, J.A., Mikić, Z.: 2009, Multispectral Emission of the Sun During the First Whole Sun Month: Magnetohydrodynamic Simulations. *Astrophys. J.* **690**, 902. [DOI](#). [ADS](#).
- Magdalenić, J., Marqué, C., Krupar, V., Mierla, M., Zhukov, A.N., Rodriguez, L., Maksimović, M., Cecconi, B.: 2014, Tracking the CME-driven Shock Wave on 2012 March 5 and Radio Triangulation of Associated Radio Emission. *Astrophys. J.* **791**, 115. [DOI](#). [ADS](#).
- Magdalenić, J., Marqué, C., Fallows, R.A., Mann, G., Vocks, C., Zucca, P., Dabrowski, B.P., Krankowski, A., Melnik, V.: 2020, Fine Structure of a Solar Type II Radio Burst Observed by LOFAR. *Astrophys. J. Lett.* **897**, L15. [DOI](#). [ADS](#).
- Mann, G., Klassen, A.: 2005, Electron beams generated by shock waves in the solar corona. *Astron. Astrophys.* **441**, 319. [DOI](#). [ADS](#).
- Mann, G., Melnik, V.N., Rucker, H.O., Konovalenko, A.A., Brazhenko, A.I.: 2018, Radio signatures of shock-accelerated electron beams in the solar corona. *Astron. Astrophys.* **609**, A41. [DOI](#). [ADS](#).
- Mann, G., Vocks, C., Warmuth, A., Magdalenić, J., Bisi, M., Carley, E., Dabrowski, B., Gallagher, P., Krankowski, A., Matyjasik, B., Rotkaehl, H., Zucca, P.: 2022, Excitation of Langmuir waves at shocks and solar type II radio bursts. *Astron. Astrophys.* **660**, A71. [DOI](#). [ADS](#).
- Mann, G., Warmuth, A., Vocks, C., Rouillard, A.P.: 2023, A heliospheric density and magnetic field model. *Astron. Astrophys.* **679**, A64. [DOI](#). [ADS](#).
- Monstein, C., Csillaghy, A., Benz, A.O.: 2023, *CALLISTO Solar Spectrogram FITS files [Data set: MEXART. Accessed on 10-Oct-2024]*, International Space Weather Initiative. [DOI](#). <https://hpde.io/ISWI/NumericalData/Callisto/FAS/PT0.25S>.
- Morosan, D.E., Carley, E.P., Hayes, L.A., Murray, S.A., Zucca, P., Fallows, R.A., McCauley, J., Kilpua, E.K.J., Mann, G., Vocks, C., Gallagher, P.T.: 2019, Multiple regions of shock-accelerated particles during a solar coronal mass ejection. *Nature Astronomy* **3**, 452. [DOI](#). [ADS](#).
- Morosan, D.E., Pomoell, J., Kumari, A., Vainio, R., Kilpua, E.K.J.: 2022, Shock-accelerated electrons during the fast expansion of a coronal mass ejection. *Astron. Astrophys.* **668**, A15. [DOI](#). [ADS](#).
- Morosan, D.E., Pomoell, J., Palmroos, C., Dresing, N., Asvestari, E., Vainio, R., Kilpua, E.K.J., Gieseler, J., Kumari, A., Jebaraj, I.C.: 2024, Connecting remote and in situ observations of shock-accelerated electrons associated with a coronal mass ejection. *Astron. Astrophys.* **683**, A31. [DOI](#). [ADS](#).
- Morosan, D.E., Dresing, N., Palmroos, C., Gieseler, J., Jebaraj, I.C., Warmuth, A., Fedeli, A., Normo, S., Pomoell, J., Kilpua, E.K.J., Zucca, P., Dabrowski, B., Krankowski, A., Mann, G., Vocks, C., Vainio, R.: 2025, Determining the acceleration regions of in situ electrons using remote radio and X-ray observations. *Astron. Astrophys.* **693**, A296. [DOI](#). [ADS](#).

- Pesce-Rollins, M., Omodei, N., Krucker, S., Di Lalla, N., Wang, W., Battaglia, A.F., Warmuth, A., Veronig, A.M., Baldini, L.: 2022, The Coupling of an EUV Coronal Wave and Ion Acceleration in a Fermi-LAT Behind-the-Limb Solar Flare. *Astrophys. J.* **929**, 172. [DOI](#). [ADS](#).
- Pesce-Rollins, M., Klein, K.-L., Krucker, S., Warmuth, A., Veronig, A.M., Omodei, N., Monstein, C.: 2024, Evidence for flare-accelerated particles in large scale loops in the behind-the-limb gamma-ray solar flare of September 29, 2022. *Astron. Astrophys.* **683**, A208. [DOI](#). [ADS](#).
- Plotnikov, I., Rouillard, A.P., Share, G.H.: 2017, The magnetic connectivity of coronal shocks from behind-the-limb flares to the visible solar surface during γ -ray events. *Astron. Astrophys.* **608**, A43. [DOI](#). [ADS](#).
- Riley, P., Lionello, R., Linker, J.A., Mikic, Z., Luhmann, J., Wijaya, J.: 2011, Global MHD Modeling of the Solar Corona and Inner Heliosphere for the Whole Heliosphere Interval. *Sol. Phys.* **274**, 361. [DOI](#). [ADS](#).
- Rodríguez-García, L., Gómez-Herrero, R., Dresing, N., Balmaceda, L.A., Palmerio, E., Kouloumvakos, A., Jebara, I.C., Espinosa Lara, F., Roco, M., Palmroos, C., Warmuth, A., Nicolaou, G., Mason, G.M., Guo, J., Laitinen, T., Cernuda, I., Nieves-Chinchilla, T., Fedeli, A., Lee, C.O., Cohen, C.M.S., Owen, C.J., Ho, G.C., Malandraki, O., Vainio, R., Rodríguez-Pacheco, J.: 2025, Solar energetic particles injected inside and outside a magnetic cloud: The widespread solar energetic particle event on 2022 January 20. *Astron. Astrophys.* **694**, A64. [DOI](#). [ADS](#).
- Rouillard, A.P., Sheeley, N.R., Tylka, A., Vourlidas, A., Ng, C.K., Rakowski, C., Cohen, C.M.S., Mewaldt, R.A., Mason, G.M., Reames, D., Savani, N.P., StCyr, O.C., Szabo, A.: 2012, The Longitudinal Properties of a Solar Energetic Particle Event Investigated Using Modern Solar Imaging. *Astrophys. J.* **752**, 44. [DOI](#). [ADS](#).
- Rouillard, A.P., Plotnikov, I., Pinto, R.F., Tirole, M., Lavarra, M., Zucca, P., Vainio, R., Tylka, A.J., Vourlidas, A., De Rosa, M.L., Linker, J., Warmuth, A., Mann, G., Cohen, C.M.S., Mewaldt, R.A.: 2016, Deriving the Properties of Coronal Pressure Fronts in 3D: Application to the 2012 May 17 Ground Level Enhancement. *Astrophys. J.* **833**, 45. [DOI](#). [ADS](#).
- Semkova, J., Koleva, R., Benghin, V., Gopalswamy, N., Matviichuk, Y., Tomov, B., Krastev, K., Maltchev, S., Dachev, T., Bankov, N., Shurshakov, V., Drobyshev, S., Mitrofanov, I., Golovin, D., Litvak, M., Sanin, A., Mokrousov, M., Lukyanov, N., Anikin, A.: 2024, Radiation environment on TGO Mars orbit during solar particle events in January–October 2024. Corresponding solar eruptions and GOES proton fluxes data. *Life Sciences in Space Research* **45**, 117. [DOI](#). [ADS](#).
- Share, G.H., Murphy, R.J., White, S.M., Tolbert, A.K., Dennis, B.R., Schwartz, R.A., Smart, D.F., Shea, M.A.: 2018, Characteristics of Late-phase \sim 100 MeV Gamma-Ray Emission in Solar Eruptive Events. *Astrophys. J.* **869**, 182. [DOI](#). [ADS](#).
- Veronig, A.M., Muhr, N., Kienreich, I.W., Temmer, M., Vršnak, B.: 2010, First Observations of a Dome-shaped Large-scale Coronal Extreme-ultraviolet Wave. *Astrophys. J. Lett.* **716**, L57. [DOI](#). [ADS](#).
- Vourlidas, A., Ontiveros, V.: 2009, A Review of Coronagraphic Observations of Shocks Driven by Coronal Mass Ejections. In: Ao, X., Burrows, G.Z.R. (eds.) *Shock Waves in Space and Astrophysical Environments: 18th Annual International AstroPhysics Conference, American Institute of Physics Conference Series* **1183**, AIP, 139. [DOI](#). [ADS](#).
- Vourlidas, A., Wu, S.T., Wang, A.H., Subramanian, P., Howard, R.A.: 2003, Direct Detection of a Coronal Mass Ejection-Associated Shock in Large Angle and Spectrometric Coronagraph Experiment White-Light Images. *Astrophys. J.* **598**, 1392. [DOI](#). [ADS](#).
- Vourlidas, A., Howard, R.A., Plunkett, S.P., Korendyke, C.M., Thernisien, A.F.R., Wang, D., Rich, N., Carter, M.T., Chua, D.H., Socker, D.G., Linton, M.G., Morrill, J.S., Lynch, S., Thurn, A., Van Duyne, P., Hagoood, R., Clifford, G., Grey, P.J., Velli, M., Liewer, P.C., Hall, J.R., DeJong, E.M., Mikic, Z., Rochus, P., Mazy, E., Bothmer, V., Rodmann, J.: 2016, The Wide-Field Imager for Solar Probe Plus (WISPR). *Space Sci. Rev.* **204**, 83. [DOI](#). [ADS](#).
- Wang, T., Reginald, N.L., Davila, J.M., St. Cyr, O.C., Thompson, W.T.: 2017, Variation in Coronal Activity from Solar Cycle 24 Minimum to Maximum Using Three-Dimensional Reconstructions of the Coronal Electron Density from STEREO/COR1. *Sol. Phys.* **292**, 97. [DOI](#). [ADS](#).
- Warmuth, A.: 2015, Large-scale Globally Propagating Coronal Waves. *Living Reviews in Solar Physics* **12**, 3. [DOI](#). [ADS](#).

-
- Wu, Y., Rouillard, A.P., Kouloumvakos, A., Vainio, R., Afanasiev, A.N., Plotnikov, I., Murphy, R.J., Mann, G.J., Warmuth, A.: 2021, On the Origin of Hard X-Ray Emissions from the Behind-the-limb Flare on 2014 September 1. *Astrophys. J.* **909**, 163. [DOI](#). [ADS](#).
- Yashiro, S., Gopalswamy, N., Michalek, G., St. Cyr, O.C., Plumkett, S.P., Rich, N.B., Howard, R.A.: 2004, A catalog of white light coronal mass ejections observed by the SOHO spacecraft. *Journal of Geophysical Research (Space Physics)* **109**, A07105. [DOI](#). [ADS](#).
- Zucca, P., Morosan, D.E., Rouillard, A.P., Fallows, R., Gallagher, P.T., Magdalenic, J., Klein, K.-L., Mann, G., Vocks, C., Carley, E.P., Bisi, M.M., Kontar, E.P., Rothkaehl, H., Dabrowski, B., Krancowski, A., Anderson, J., Asgekar, A., Bell, M.E., Bentum, M.J., Best, P., Blaauw, R., Breitling, F., Broderick, J.W., Brouw, W.N., Briggen, M., Butcher, H.R., Ciardi, B., de Geus, E., Deller, A., Duscha, S., Eisloeffel, J., Garrett, M.A., Grießmeier, J.M., Gunst, A.W., Heald, G., Hoeft, M., Hörandel, J., Iacobelli, M., Juette, E., Karastergiou, A., van Leeuwen, J., McKay-Bukowski, D., Mulder, H., Munk, H., Nelles, A., Orru, E., Paas, H., Pandey, V.N., Pekal, R., Pizzo, R., Polatidis, A.G., Reich, W., Rowlinson, A., Schwarz, D.J., Shulevski, A., Sluman, J., Smirnov, O., Sobey, C., Soida, M., Thoudam, S., Toribio, M.C., Vermeulen, R., van Weeren, R.J., Wucknitz, O., Zarka, P.: 2018, Shock location and CME 3D reconstruction of a solar type II radio burst with LOFAR. *Astron. Astrophys.* **615**, A89. [DOI](#). [ADS](#).